



## Article

# Red Blood Cell BCL-x<sub>L</sub> Is Required for *Plasmodium falciparum* Survival: Insights into Host-Directed Malaria Therapies

Coralie Boulet <sup>1,†</sup> , Ghizal Siddiqui <sup>2</sup>, Taylah L. Gaynor <sup>1,‡</sup>, Christian Doerig <sup>3</sup>, Darren J. Creek <sup>2</sup>   
and Teresa G. Carvalho <sup>1,\*</sup>

- <sup>1</sup> Department of Microbiology, Anatomy, Physiology and Pharmacology, School of Agriculture, Biomedicine and Environment, La Trobe University, Bundoora, VIC 3086, Australia; coralie.boulet@burnet.edu.au (C.B.); 18498207@students.latrobe.edu.au (T.L.G.)
- <sup>2</sup> Monash Institute of Pharmaceutical Sciences, Monash University, Parkville, VIC 3052, Australia; ghizal.siddiqui@monash.edu (G.S.); darren.creek@monash.edu (D.J.C.)
- <sup>3</sup> School of Health and Biomedical Sciences, RMIT University, Bundoora, VIC 3083, Australia; christian.doerig@rmit.edu.au
- \* Correspondence: t.carvalho@latrobe.edu.au
- † Present address: Burnet Institute, Melbourne, VIC 3004, Australia.
- ‡ Present address: Baker Heart and Diabetes Research Institute, Melbourne, VIC 3004, Australia.

**Abstract:** The development of antimalarial drug resistance is an ongoing problem threatening progress towards the elimination of malaria, and antimalarial treatments are urgently needed for drug-resistant malaria infections. Host-directed therapies (HDT) represent an attractive strategy for the development of new antimalarials with untapped targets and low propensity for resistance. In addition, drug repurposing in the context of HDT can lead to a substantial decrease in the time and resources required to develop novel antimalarials. Host BCL-x<sub>L</sub> is a target in anti-cancer therapy and is essential for the development of numerous intracellular pathogens. We hypothesised that red blood cell (RBC) BCL-x<sub>L</sub> is essential for *Plasmodium* development and tested this hypothesis using six BCL-x<sub>L</sub> inhibitors, including one FDA-approved compound. All BCL-x<sub>L</sub> inhibitors tested impaired proliferation of *Plasmodium falciparum* 3D7 parasites *in vitro* at low micromolar or sub-micromolar concentrations. Western blot analysis of infected cell fractions and immunofluorescence microscopy assays revealed that host BCL-x<sub>L</sub> is relocated from the RBC cytoplasm to the vicinity of the parasite upon infection. Further, immunoprecipitation of BCL-x<sub>L</sub> coupled with mass spectrometry analysis identified that BCL-x<sub>L</sub> forms unique molecular complexes with human μ-calpain in uninfected RBCs, and with human SHOC2 in infected RBCs. These results provide interesting perspectives for the development of host-directed antimalarial therapies and drug repurposing efforts.

**Keywords:** BCL-x<sub>L</sub>; malaria; *Plasmodium falciparum*; host-directed therapy; red blood cells; host–parasite interaction



**Citation:** Boulet, C.; Siddiqui, G.; Gaynor, T.L.; Doerig, C.; Creek, D.J.; Carvalho, T.G. Red Blood Cell BCL-x<sub>L</sub> Is Required for *Plasmodium falciparum* Survival: Insights into Host-Directed Malaria Therapies. *Microorganisms* **2022**, *10*, 824. <https://doi.org/10.3390/microorganisms10040824>

Academic Editors: Ana Paula Arez and Marcia Medeiros

Received: 28 March 2022

Accepted: 13 April 2022

Published: 15 April 2022

**Publisher's Note:** MDPI stays neutral with regard to jurisdictional claims in published maps and institutional affiliations.



**Copyright:** © 2022 by the authors. Licensee MDPI, Basel, Switzerland. This article is an open access article distributed under the terms and conditions of the Creative Commons Attribution (CC BY) license (<https://creativecommons.org/licenses/by/4.0/>).

## 1. Introduction

Malaria is a vector-borne parasitic infection caused by apicomplexan parasites of the genus *Plasmodium*, of which *Plasmodium falciparum* causes the most severe forms of disease. Malaria remains an ongoing and significant global health threat in the 21st century. Recently, disruptions caused by the COVID-19 pandemic further increased the impact of malaria, with 241 million cases and 627,000 deaths in 2020 (a 12% increase compared to 2019 [1]). Despite significant efforts made towards malaria control in recent decades, many formidable challenges stand in the way of the elimination of malaria [2]. This includes the emergence and spread of drug resistance, the low efficacy of the recently approved malaria vaccine [3,4], the impact of the climate crisis on health care systems and vector distribution, and additional pandemics. Worryingly, reduced susceptibility of parasites to the current frontline treatment, artemisinin-combination therapies (ACTs), is also observed [5].

*P. falciparum* initially invades and replicates inside liver cells, but disease symptoms and deaths associated with malaria are caused by the subsequent parasite replication inside red blood cells (RBCs); therefore, most current antimalarials target blood-stage parasite molecules. Noteworthy, as drug resistant parasites develop against all existing antimalarial treatments, host-directed therapies (HDT) emerge as a novel and promising antimalarial strategy for two main reasons [6,7]. Firstly, targeting host molecules that are required for the development of *Plasmodium* limits the most straightforward pathway for drug resistance (i.e., mutation of the target molecule). Secondly, many drugs targeting human molecules already exist in the context of other diseases such as cancers [8] and may be repurposed for antimalarial treatment, therefore saving time and resources required for drug development.

In this perspective, host programmed cell death pathways represent potential anti-parasitic targets. This is because apicomplexan parasites, including *Plasmodium* spp., are known to manipulate the host cell death pathways to allow their own intracellular survival [9,10]. Further, many compounds targeting cell death pathways are available and are clinically approved for the treatment of other human diseases [8]. Importantly, this host-directed strategy has proven effective against *Plasmodium* parasites: ABT-737, an inhibitor of the anti-apoptotic members of the BCL-2 (B-cell lymphoma 2) family BCL-2 and BCL-x<sub>L</sub>, was shown to eliminate liver stages of *Plasmodium* spp. both *in vitro* and in murine models [11]. Importantly, no *bcl-2* or *bcl-x<sub>L</sub>* orthologs have been identified in *Plasmodium* spp., suggesting that the effect observed was due to the inhibition of the host molecules (although parasite-encoded off-targets cannot be excluded at this stage). RBCs are devoid of mitochondria and are therefore unable to undergo classical apoptosis. However, BCL-x<sub>L</sub> has been identified in proteomics studies of RBCs [12], and its inhibition induces eryptosis, the programmed cell death of RBCs [13,14].

The present study investigates the impact of six BCL-x<sub>L</sub> inhibitors on the proliferation of *P. falciparum* *in vitro* and on RBCs death. The six BCL-x<sub>L</sub> inhibitors include one FDA-approved drug and have been selected based on their target specificity, clinical use, and/or ongoing clinical trials. Further, the localization and binding partners of RBC BCL-x<sub>L</sub> were determined in *P. falciparum*-infected RBCs (iRBCs) and uninfected RBCs (uRBCs). All BCL-x<sub>L</sub> inhibitors impaired *P. falciparum* growth *in vitro* (some with submicromolar IC<sub>50</sub> values) and induced eryptosis of iRBCs. Moreover, in iRBCs, BCL-x<sub>L</sub> was recruited to the vicinity of the parasite and appeared to form unusual complexes, with a shift in binding partners (compared to uRBCs) upon infection. Notably, we show that BCL-x<sub>L</sub> binds to  $\mu$ -calpain in uRBCs and to the human SHOC2 leucine rich repeat scaffold protein in iRBCs. These observations raise fascinating questions regarding the role of BCL-x<sub>L</sub> in RBCs in general, and, more crucially, during *Plasmodium* infection. Overall, these results provide exciting perspectives regarding host-directed antimalarial therapies and drug-repurposing opportunities.

## 2. Materials and Methods

### 2.1. *P. falciparum* Culture

*P. falciparum* 3D7 parasites were cultured *in vitro* with human RBCs (kindly donated by the Australian Red Cross) as previously described [15]. Briefly, parasites were cultured at 4% haematocrit in complete RPMI (cRPMI: 16.2 g/L RPMI 1640 Medium HEPES, 50 mg/L hypoxanthine, 10 mg/L gentamicin, 2.25 g/L sodium bicarbonate, 5 g/L AlbuMAX lipid-rich BSA), and incubated at 37 °C in 1% O<sub>2</sub>, 5% CO<sub>2</sub>, and 94% N<sub>2</sub>. This work was supported by an Australian Red Cross Blood Service Agreement (19-05VIC-01) and approved by the La Trobe University Research Ethics Committee (HEC17-013).

### 2.2. Growth Inhibition Assays (IC<sub>50</sub>)

Growth inhibition assays were conducted as previously described [16] for the following BCL-x<sub>L</sub> inhibitors (Table 1): ABT-737 (Sapphire Bioscience #A10255), ABT-263 (Sapphire Bioscience #A10022), ABT-199 (Sapphire Bioscience #A12500), WEHI-539 (Sapphire Bioscience #S7100), A-1155463 (Sapphire Bioscience #S7800), and A-1331852 (Sapphire

Bioscience #S7801). Asynchronous parasite stages were exposed to 0.2 nM–50  $\mu$ M of compound for 72 h. Artemisinin (ART) and chloroquine (CQ) (both at 50  $\mu$ M) served as a growth inhibition positive control, and DMSO as a negative control. Following a freeze–thaw cycle, parasite DNA was stained with the fluorescent nucleic acid dye SYBR Gold (Invitrogen), and fluorescence was measured on a CLARIOstar<sup>®</sup> microplate reader. Data were transformed in Excel using the formula below (“averageFluo” refers to the average fluorescence over technical triplicates), and percent inhibition was graphed against the logarithm of concentration using GraphPad Prism<sup>®</sup> 8 software. Data are shown as the mean  $\pm$  SD of 3 independent replicates, and the half-maximal inhibitory concentration (IC<sub>50</sub>) is indicated.

$$\frac{\text{averageFluo}(\text{sample}) - \text{averageFluo}(\text{DMSO})}{\text{averageFluo}(\text{ART\&CQ}) - \text{averageFluo}(\text{DMSO})} * 100$$

### 2.3. Immunofluorescence Assay (IFA)

Cells from an asynchronous culture at high parasitemia (>5%) were fixed for 30 min in 4% paraformaldehyde and 0.0075% glutaraldehyde. Following membrane permeabilization with 0.1% Triton X-100 for 10 min at room temperature, cells were blocked with 3% Bovine Serum Albumin (BSA) overnight at 4 °C and incubated successively with primary and secondary antibodies, overnight at 4 °C and 1 h at room temperature, respectively. Cells were mixed with VectaShield containing DAPI (2  $\mu$ g/mL) and imaged on a Zeiss Axioscope microscope using an Orca Digitalcamera (1000 magnification).

### 2.4. Flow Cytometry Assay

RBC death was assessed by flow cytometry, measuring the exposure of phosphatidylserine (PS) on the cell surface as previously established [16]. Briefly, asynchronous *P. falciparum* cultures and uRBCs were incubated with a BCL-x<sub>L</sub> inhibitor (5  $\mu$ M for compounds with a *P. falciparum* IC<sub>50</sub> < 5  $\mu$ M, and 10  $\mu$ M for the others) for 4 h in incomplete RPMI (iRPMI; media without Albumax and sodium bicarbonate) at 37 °C under low-oxygen conditions. BCL-x<sub>L</sub> inhibitors were removed by washing cells once with Phosphate-Buffered Saline (PBS), and parasite RNA and DNA were stained for 40 min with 4  $\mu$ M Hoechst 33342 in Thiazole Orange (BD ReticCount<sup>™</sup>). Cells were washed in staining buffer (5 mM CaCl<sub>2</sub>, 5 mM glucose, 32 mM HEPES pH 7.4, 5 mM KCl, 1 mM MgSO<sub>4</sub>, 125 mM NaCl) and incubated for 20 min with Annexin V-PE (1:20 dilution in staining buffer; BD Bioscience) for the staining of surface-exposed PS. A total of 100,000 events were recorded on a CytoFLEX S flow cytometer (Beckman Coulter, Brea, CA, USA), and data were analysed using FlowJo V10.

### 2.5. Fractionation of Parasite and RBC Proteins

**Trophozoite-iRBC enrichment.** *P. falciparum* cultures were synchronized to ring-stage parasites by sorbitol treatment as previously described [17] and allowed to mature into trophozoites for 24 h. Magnetic separation (VarioMACS<sup>™</sup> Separator, Miltenyi Biotec, Bergisch Gladbach, Germany) was used to purify the trophozoite-stage parasites as described previously [18]. Briefly, trophozoite cultures were loaded on an CS Column (Miltenyi Biotec, Bergisch Gladbach, Germany) previously equilibrated with iRPMI and then abundantly washed with iRPMI. The column was detached from the VarioMACS, and magnet-bound parasites were eluted into a clean tube with cRPMI. The efficiency of trophozoite enrichment was assessed by a thin blood smear.

**Total protein extraction.** Cell numbers were determined with a haemocytometer (Merck, Darmstadt, Germany). Cell lysis of 10<sup>8</sup> uRBCs and 10<sup>8</sup> magnet-purified iRBCs was achieved by incubation with 80  $\mu$ L of M-PER<sup>™</sup> (ThermoFisher, Waltham, MA, USA) supplemented with protease and phosphatase inhibitors (PPI) (1X Protease Inhibitors Cocktail EDTA-free (Roche, Basel, Switzerland), 20 mM sodium fluoride, 100  $\mu$ M sodium orthovanadate, 1 mM PMSF, 10 mM  $\beta$ -glycerophosphate) on ice for 10 min, and TALON<sup>®</sup> Metal Affinity Resin (Takara, Kusatsu, Japan) was used to remove the haemoglobin, as

described previously [19]. Briefly, 100  $\mu\text{L}$  of resin were incubated with the cell lysate for 10 min at 4 °C. Following centrifugation, the supernatant (i.e., haemoglobin-depleted protein sample) was collected, denatured with Laemmli Buffer for 5 min at 98 °C, and stored at  $-20$  °C.

**RBC cytosolic protein vs. membrane-bound and parasite protein extraction.** Saponin is a gentle detergent that solubilizes the RBC and the parasitophorous vacuole membranes but not the parasite plasma membrane [20]. Therefore, in iRBCs, proteins localized in the RBC cytosol were separated from the fraction containing the parasite and the membrane-bound proteins through a saponin lysis. Similarly, in uRBCs, cytosolic proteins were separated from membrane proteins with the same process. Magnet-purified iRBCs and uRBCs ( $10^8$  cells) were incubated with 0.1% saponin-PPI on ice for 10 min, then centrifuged for 5 min at  $16,200\times g$  at 4 °C. The soluble fraction (i.e., supernatant) was collected, haemoglobin-depleted with TALON resin, denatured with Laemmli Buffer for 5 min at 98 °C, and stored at  $-20$  °C (see above). The insoluble fraction (i.e., pellet of the saponin lysis, containing the parasite and membrane proteins fraction) was lysed again with 0.1% saponin-PPI on ice for 10 min, then centrifuged for 5 min at maximum speed at 4 °C. To ensure removal of haemoglobin and other RBC cytosolic proteins, the resulting pellet was washed with PBS-PPI. Samples were denatured in Laemmli Buffer for 5 min at 98 °C and stored at  $-20$  °C.

## 2.6. Western Blot Analysis

Protein extracts of  $10^7$  of either uRBCs or iRBCs and of the breast cancer cell line MDA-MB 231 (used as a positive control and kindly provided by Dr. Delphine Merino, Olivia Newton-John Cancer Research Centre) were loaded on a 4–12% Bis-Tris gel (Novex™) and resolved in MES-SDS running buffer (Novex™). Proteins were transferred onto a 0.2  $\mu\text{m}$  nitrocellulose membrane (BioRad, Hercules, CA, USA) in transfer buffer (0.3% Tris base, 0.75% glycine, 20% methanol), and the membrane was washed in PBST (0.1% Tween-20 in PBS) for 10 min and then blocked overnight at 4 °C in 5% milk-PBST. Primary and secondary antibodies were incubated successively, overnight at 4 °C and for 1 h at room temperature, respectively. Dilutions of primary antibodies (in 5% BSA-PBST) were used as follows: BCL- $x_L$  1:1000 (Cell Signaling, Danvers, MA, USA, #2764), Carbonic Anhydrase 1:4000 (Abcam, Cambridge, UK, #ab108367), PfHSP70.1 1:5000 (kindly provided by Prof Gilson and Prof Crabb, Burnet Institute), and protein 4.1 1:500 (kindly provided by Dr. Proellocks and Prof Cooke, Monash University). Secondary antibody: anti-rabbit-HRP 1:5000 (Cell Signaling, #7074). HRP signal was revealed with Pierce™ ECL Western Blotting Substrate (Thermo Scientific) and detected with a ChemiDoc XRS+ system.

## 2.7. Immunoprecipitation of Host BCL- $x_L$

**Sample preparation.** Magnet-purified trophozoite-iRBCs and uRBCs ( $10^9$  cells) were incubated with either 10  $\mu\text{M}$  WEHI-539 or DMSO for 4 h at 37 °C in low-oxygen conditions. Cells were lysed with 800  $\mu\text{L}$  M-PER™-PPI for 15 min as described above.

**Immunoprecipitation of BCL- $x_L$ .** Protein A magnetic beads (Gen-Script, Piscataway, NJ, USA) were pre-incubated with anti-BCL- $x_L$  antibody (1:100, Cell Signaling, #2764) in TBST (20 mM Tris, 150 mM NaCl, 0.1% Tween-20) overnight at 4 °C under gentle agitation. Magnetic beads were incubated in TBST without antibody for the control (beads alone). Unbound antibody was removed with a TBST-PPI wash, and protein extracts were added to the beads and incubated overnight at 4 °C under gentle agitation. Unbound proteins were removed with TBST-PPI washing. BCL- $x_L$  bound proteins were solubilized following resuspension of the washed beads in Laemmli buffer for 5 min at 95 °C. Samples were kept at  $-20$  °C before mass spectrometry analysis. The presence of BCL- $x_L$  in the immunoprecipitates was confirmed by Western Blot analysis of 1/10th of each sample.

### 2.8. Mass Spectrometry Analysis of the BCL-x<sub>L</sub> Immunoprecipitates

**Mass spectrometry.** The BCL-x<sub>L</sub> immunoprecipitated samples (i.e., BCL-x<sub>L</sub>-coated magnetic beads and bound proteins) were resolved on a 1D PAGE gel (Mini-PROTEAN<sup>®</sup> TGXTM, Bio-Rad) at 200 V for 5 min and proteins were fixed on gels with Instant Blue stain (Abcam, Cambridge, UK). Following gel destaining with MilliQ water, the entire area of protein migration was excised and subjected to in-gel trypsin digestion, as previously described [21]. Peptides were extracted, dried in a Speed-Vac, subjected to desalting as previously described [21], and reconstituted in 12 µL of 2% acetonitrile (ACN), 0.1% formic acid for mass spectrometry analysis. Liquid chromatography with tandem mass spectrometry (LC-MS/MS) analysis was carried out as previously described with minor modifications [22]. For label-free proteomics analysis, the HPLC gradient was set to 98 min using a gradient that reached 30% ACN after 63 min, 34% after 66 min, and 79.2% after 71 min, following which there was an equilibration phase of 20 min at 2% ACN. Peptide sequences and protein identity were determined using MaxQuant software (version 1.6.0.1) by matching protein database of *P. falciparum* (UP000001450, release version 2016 04) and *Homo sapiens* (UP000005640, release version 2017 05) [21].

**Data analysis.** The outputs from MaxQuant were filtered to remove known contaminants, reverse sequences, and proteins identified by a single site. Protein identification FDR was as per default parameters of 0.01 [21], and label-free quantification was enabled. Match between run option was not enabled so that false positives would not be identified. Only proteins detected in at least 2 out of 3–5 biological replicates of uRBC- and iRBC-immunoprecipitated (IP) samples were considered for analysis. Proteins identified in the uRBC-IP or iRBC-IP samples and in the beads-only controls were excluded from the analysis. Interacting partners were based on the number of independent replicates the protein was identified in (2 or more) and the average intensities across all replicates for the specific proteins, which had to be greater than the treated (+inhibitor) samples (Tables 2 and 3). Of note, the relative intensity was used, not the normalized intensity [23], and the average did not include zero intensities in the case where no peptide was identified in a replicate.

## 3. Results

### 3.1. BCL-x<sub>L</sub> Inhibitors Impair *P. falciparum* Proliferation

Six BCL-x<sub>L</sub> inhibitors, selected based on their target specificity and/or current clinical use (Table 1), were tested in *in vitro* parasite proliferation inhibition assays. The selected BCL-x<sub>L</sub> inhibitors include ABT-199 (Venclexta<sup>™</sup>, Venclyxto, Venetoclax), an FDA-approved compound for the treatment of leukaemia, and ABT-263 (Navitoclax), a compound currently in phase I/II clinical trials for the treatment of lymphoid malignancies. All six compounds significantly affected *P. falciparum* proliferation *in vitro*, as illustrated by the measured low IC<sub>50</sub> values (Figure 1). ABT-263 and WEHI-539 displayed the lowest IC<sub>50</sub> values of 0.74 and 0.82 µM, respectively, while A-1155463, ABT-199 and ABT-737 IC<sub>50</sub> values were measured between 4 and 7 µM (4.23, 4.6 and 6.57 µM, respectively). A-1331852 presented the highest IC<sub>50</sub> value at 14.05 µM.

**Table 1. BCL-x<sub>L</sub> inhibitors tested for inhibition of *P. falciparum* viability in this study.** The compound's molecular target(s), current phase of clinical development, and clinical purpose are indicated. The reported activity of the compounds on *Plasmodium* liver stages is reported when available. The IC<sub>50</sub> measured for each compound on *P. falciparum* blood stage in this study is reported (see Figure 1 for details). K<sub>i</sub>: inhibitory constant (reflective of the compound binding affinity).

Compound	Molecular Target	Human		<i>Plasmodium</i>		
		Clinical Development	Clinical Use	Peak Plasma Levels	Activity on Liver Stages	IC <sub>50</sub> on Blood Stages (This Study)
ABT-263 (Navitoclax)	BCL-2~BCL-x~BCL-w (K <sub>i</sub> < 1 nM) [24]	Phase I/II [24]	lymphoid malignancies; Chronic lymphocytic leukaemia [24]	~5.75 μM [25]	No [26]	0.74 μM
WEHI-539	BCL-x <sub>L</sub> (IC <sub>50</sub> = 1.1 nM) [27]	Pre-clinical [27]	N/A (poor physicochemical properties) [27]	N/A	N/A	0.82 μM
A-1155463	BCL-x <sub>L</sub> (K <sub>i</sub> < 0.01 nM) [28]	Pre-clinical [28]	N/A	N/A	N/A	4.23 μM
ABT-199 (Venclexta™, Venclyxto, Venetoclax)	BCL-2 (K <sub>i</sub> < 0.01 nM) BCL-x <sub>L</sub> ; BCL-w (K <sub>i</sub> < 48 nM; <245 nM) [29]	FDA approved (2016)	Chronic lymphocytic leukaemia	~3.45 μM [30]	N/A	4.6 μM
ABT-737	BCL-2~BCL-x <sub>L</sub> ~BCL-w (K <sub>i</sub> < 1 nM) [31]	No	N/A (low solubility and bioavailability) [31]	N/A	Yes [11]	6.57 μM
A-1331852	BCL-x <sub>L</sub> (K <sub>i</sub> < 0.01 nM) BCL-w; BCL-2 (K <sub>i</sub> = 4 nM; 6 nM) [32]	Pre-clinical [32]	N/A	N/A	N/A	14.05 μM

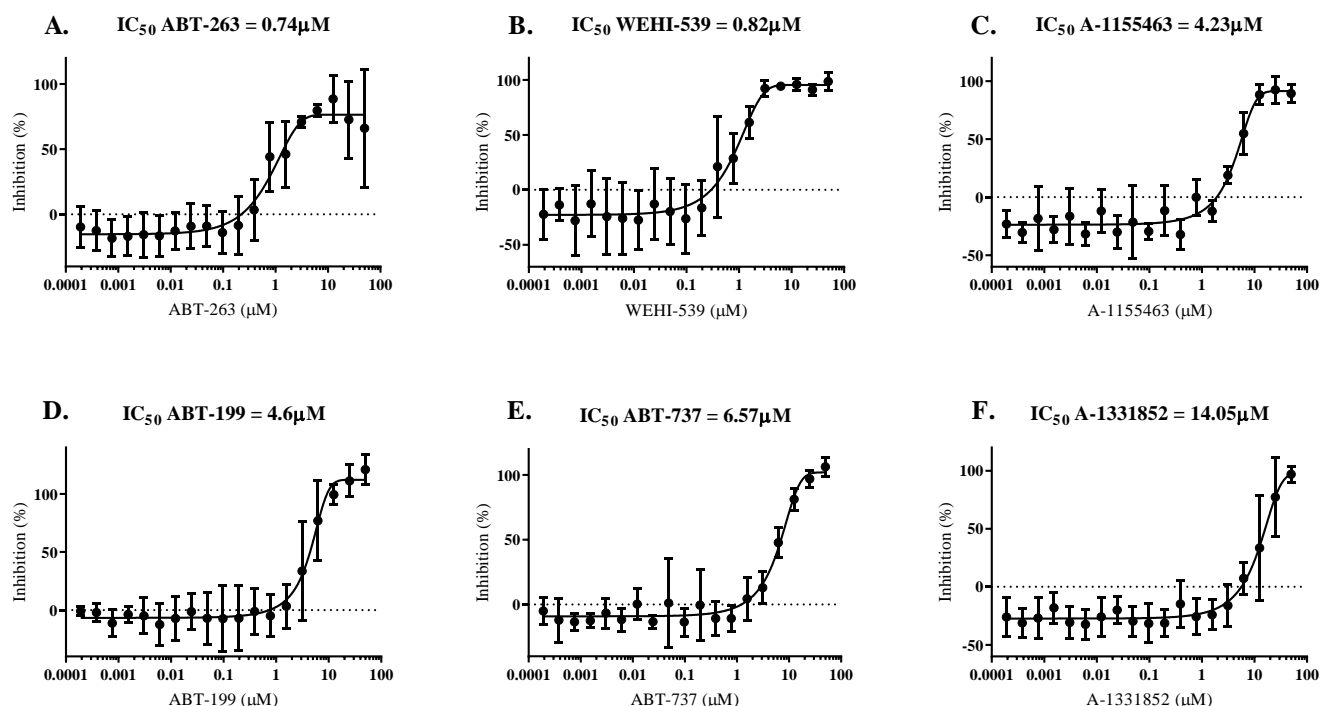


**Figure 1. Impact of BCL-x<sub>L</sub> inhibitors on *P. falciparum* growth *in vitro*.** (A) ABT-263. (B) WEHI-539. (C) A-1155463. (D) ABT-199. (E) ABT-737. (F) A-1331852. Growth assays of six BCL-x<sub>L</sub> inhibitors were conducted over 72 h on an asynchronous parasite culture, and the IC<sub>50</sub> was calculated based on three independent biological replicates ( $n = 3$ , mean  $\pm$  SD).

### 3.2. BCL-x<sub>L</sub> Inhibitors Induce Eryptosis of uRBCs and iRBCs

RBCs do not possess a classical apoptotic pathway due to the lack of a mitochondrion and a nucleus. Instead, they display a form of programmed cell death termed eryptosis [14]. Little is known about the molecular events leading to eryptosis, but a major hallmark of RBC death is the exposure of phosphatidylserine (PS) at the cell surface [33]. To test the ability of BCL-x<sub>L</sub> inhibitors to induce eryptosis, we exposed uRBCs and *P. falciparum*-iRBCs to six BCL-x<sub>L</sub> inhibitors (Table 1) for 4 h according to previously established guidelines [16], and RBC surface exposure of PS was measured by flow cytometry (Figure 1; treatment was with 5 μM or 10 μM of BCL-x<sub>L</sub> inhibitor, depending on whether their IC<sub>50</sub> was below or greater than 1 μM, respectively). A significant increase in the percentage of PS-exposing cells was observed in uRBCs in the presence of WEHI-539, A-1155463, and A-1331852 when compared with the respective no drug control. An increase in the percentage of PS-exposing cells was also observed in iRBCs in the presence of all six BCL-x<sub>L</sub> inhibitors, albeit not significantly for ABT-737 (Figure 2). These results suggest that the inhibition of BCL-x<sub>L</sub> induces eryptosis in uRBCs as well as in iRBCs.

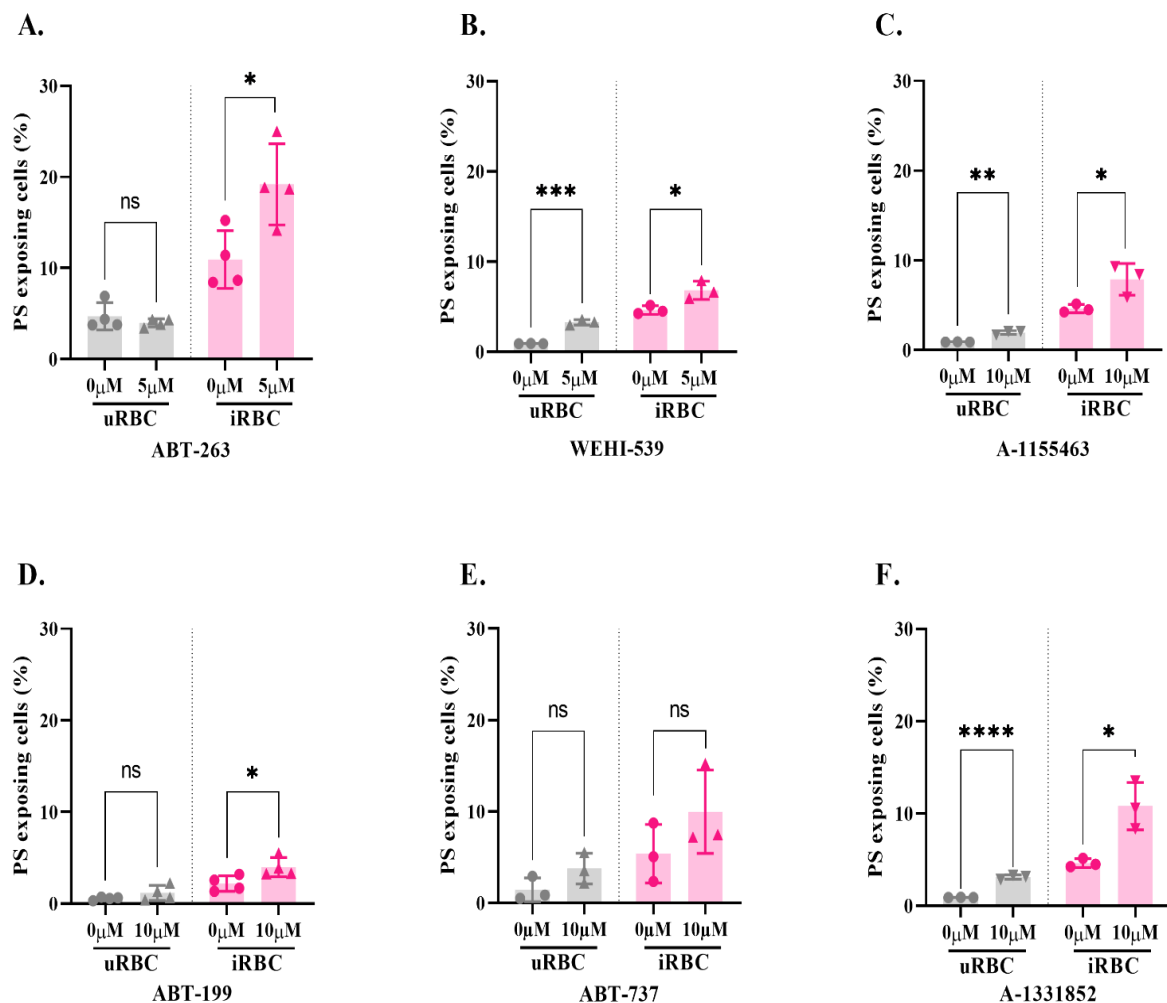


**Figure 2.** PS exposure of uRBCs and iRBCs exposed to BCL-x<sub>L</sub> inhibitors. (A) ABT-263. (B) WEHI-539. (C) A-1155463. (D) ABT-199. (E) ABT-737. (F) A-1331852. iRBC or uRBC cultures were exposed to 5 or 10 μM of BCL-x<sub>L</sub> inhibitors for 4 h in incomplete RPMI (following previously established guidelines [16]). The percentage of PS exposing cells was measured by flow cytometry (iRBCs were detected using a DNA stain). Individual values of  $n = 3-4$  independent experiments (in technical duplicates) are shown, along with the mean  $\pm$  SD. Unpaired  $t$ -tests were conducted (\*\*\*\*:  $p \leq 0.0001$ ; \*\*\*:  $p \leq 0.001$ ; \*\*:  $p \leq 0.01$ ; \*:  $p \leq 0.05$ ).

### 3.3. Host BCL-x<sub>L</sub> Is Recruited to the Parasite

In nucleated cells, the role of BCL-x<sub>L</sub> in apoptosis is intrinsically dependent on its cellular localization, either at the mitochondria outer membrane or in the cytosol [34]. Therefore, the subcellular localization of BCL-x<sub>L</sub> was investigated in iRBCs and uRBCs by Western blot and IFA (Figure 3).

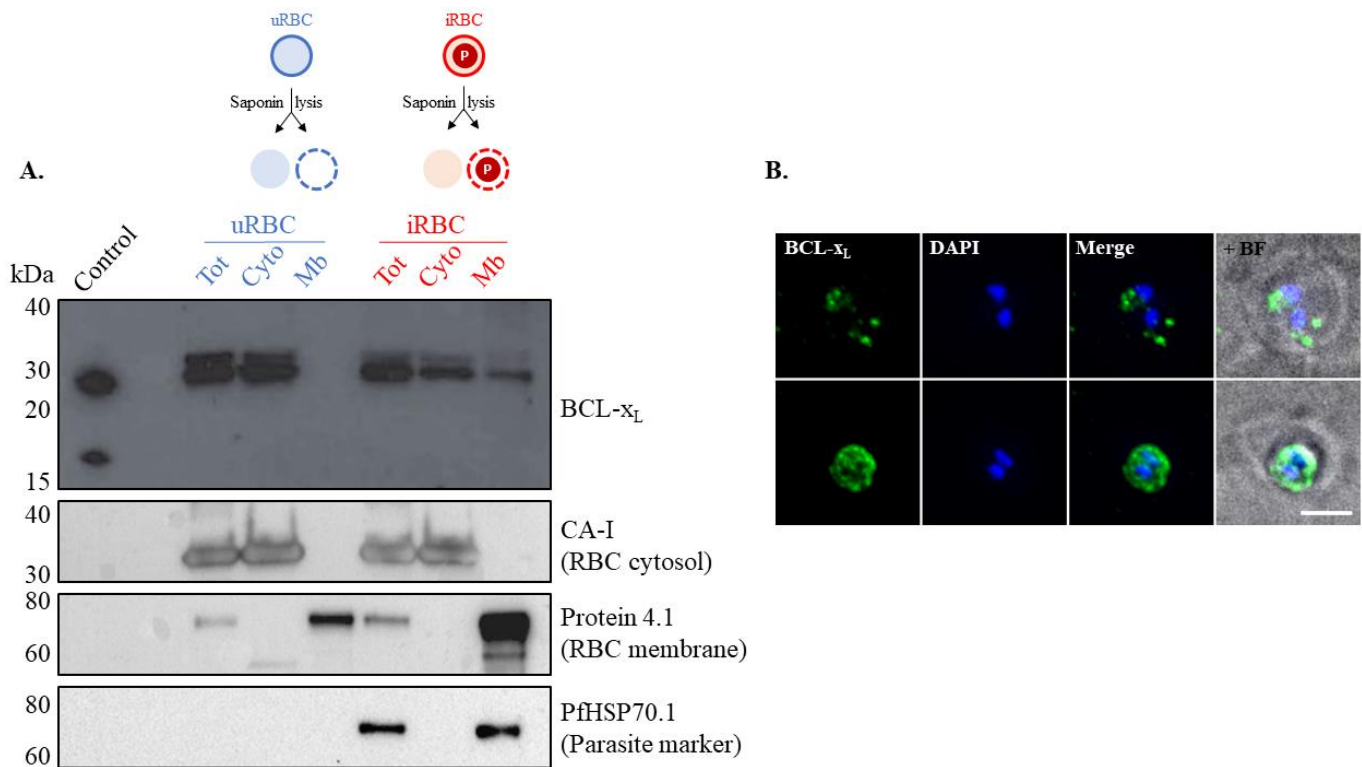


**Figure 3.** Subcellular localization of BCL-x<sub>L</sub> in uRBCs and iRBCs. (A) Representative Western blot of uRBCs or iRBCs: total protein extraction (tot), cytosolic content (cyto—soluble fraction of a saponin lysis), and membrane fraction (Mb—insoluble fraction of a saponin lysis). BCL-x<sub>L</sub> localizes exclusively to the cytosolic fraction in uRBCs and to the cytosolic and membrane fractions in iRBCs. A 16 kDa band corresponding to cleaved BCL-x<sub>L</sub> is observed in the control but not in the uRBC and iRBC fractions. The control sample corresponds to protein extracts derived from the breast cancer cell line MDA-MB 231. The same blot was successively probed with the following antibodies: anti-BCL-x<sub>L</sub>, anti-Carbonic Anhydrase I (CA-I), anti-protein 4.1, and anti-PfHSP70.1. CA-I, Protein 4.1, and PfHSP70 are markers for the RBC cytosol, the RBC membrane, and the parasite, respectively. Note: control panels are also used in another study focussing on the protein BAD (to be published elsewhere) (B) Immunofluorescence assay of iRBCs (two representative cells are shown: early and mid-stage of infection in the upper and lower panels, respectively). BCL-x<sub>L</sub> (green) is detected in the vicinity of the parasite, outside of the nucleus area stained with DAPI (blue) and inside the RBC membrane, which is visible by Bright Field (BF). The scale bar is 4 μm.

Western blot analysis of saponin-lysed cells (see Figure 3A for a representative example) revealed the presence of BCL-x<sub>L</sub> in the cytosol of uRBCs and iRBCs. However, BCL-x<sub>L</sub> was also found in the membrane fraction of iRBCs, suggesting its association with the RBC plasma membrane, the parasitophorous vacuole membrane, the parasitophorous vacuole compartment, the parasite plasma membrane, and/or the parasite itself. The effectiveness of the cell lysis assay and control for protein leakage between the cytosolic and the membrane compartments was assessed with various antibody controls to detect RBCs cytosolic and membrane proteins, carbonic anhydrase I (CA-I), and protein 4.1, respectively. CA-I, a highly abundant cytosolic enzyme of RBCs [35], was detected in the cytosolic fractions of iRBCs and uRBCs but not in the membrane fractions, demonstrating that the membrane

fractions were not contaminated with cytosolic proteins. Similarly, the major cytoskeletal protein of uRBCs, protein 4.1 [36], was detected in the membrane fractions of both uRBCs and iRBCs, but not in the cytosolic fractions, demonstrating that the cytosolic fractions were not contaminated with membrane or parasite proteins. Further, the absence of the *P. falciparum* protein PfHSP70.1 [37] in the uRBC fraction and in the RBC cytoplasm of infected cells indicated that parasite proteins do not contaminate the latter fraction. Of note, the signal of protein 4.1 was stronger in the membrane fraction compared to the total fraction in both uRBCs and iRBCs (although more striking in the iRBC sample). However, the signals of CA-I and PfHSP70.1 were consistent across the samples, confirming that equivalent amounts of proteins were loaded in each lane.

To gain further insight into the cellular localization of BCL-x<sub>L</sub> in iRBCs, an IFA was performed using a human anti-BCL-x<sub>L</sub> antibody. The BCL-x<sub>L</sub> fluorescent signal produced was associated with the parasite, while BCL-x<sub>L</sub> was not detected at the RBC membrane or in the cytosol of iRBCs (Figure 3B). In summary, we conclude that host BCL-x<sub>L</sub> localizes to the uRBCs cytosol and is recruited to the vicinity of the parasite upon *P. falciparum* infection (see Discussion).

### 3.4. BCL-x<sub>L</sub> Can Be Immunoprecipitated from uRBCs and iRBCs Cellular Extracts

In nucleated cells, the nature of the molecular complexes formed by BCL-x<sub>L</sub> with different binding partners determines its pro- or anti-apoptotic activity. Typically, binding of BCL-x<sub>L</sub> to the pore-forming proteins BAX and BAK leads to anti-apoptotic activity, whereas binding of BCL-x<sub>L</sub> to the protein BAD leads to a pro-apoptotic outcome [38]. Interactors of BCL-x<sub>L</sub> in RBCs have not been investigated to date. BCL-x<sub>L</sub> from uRBCs and iRBCs was immunoprecipitated (IP) using a human anti-BCL-x<sub>L</sub> antibody, and mass spectrometry was used to analyse the immunoprecipitated proteins (IP). To ensure the specificity of the BCL-x<sub>L</sub> complexes, the BCL-x<sub>L</sub> inhibitor WEHI-539 was used. Indeed, WEHI-539 has been shown to inhibit BCL-x<sub>L</sub> in nucleated cells by displacing its binding partners from the BH3 domain-binding groove [27]. To test the hypothesis that WEHI-539 induces a similar displacement of BCL-x<sub>L</sub> molecular complexes in uRBCs and iRBCs, cells were incubated with WEHI-539 (or with the control vehicle DMSO) prior to immunoprecipitation with an anti-BCL-x<sub>L</sub> antibody coupled to Western blot and mass spectrometry analyses. (Supplementary Tables S4 and S5). Cellular extracts incubated with beads alone (without antibody) were used as negative controls.

Western blot analysis of the BCL-x<sub>L</sub> immunoprecipitates revealed the successful pull-down of BCL-x<sub>L</sub> in the IP samples of uRBCs and iRBCs, in the presence and absence of the BCL-x<sub>L</sub> inhibitor WEHI-539 (uRBC-IP +/– inhibitor, iRBC-IP +/– inhibitor; Supplementary Figure S1). BCL-x<sub>L</sub> was not detected in the negative controls (i.e., material recovered from beads alone, without BCL-x<sub>L</sub> antibody) of uRBC and iRBC samples.

Mass spectrometry analysis of the BCL-x<sub>L</sub> immunoprecipitates identified seven peptides (from 7 to 29 amino acids) from the human protein BCL2-L1 (Supplementary Table S1 and Supplementary Figure S2). Differential splicing of the *bcl2-l1* gene can produce either BCL-x<sub>L</sub> or BCL-x<sub>S</sub> proteins. BCL-x<sub>S</sub> lacks amino acids 127 to 187 of BCL-x<sub>L</sub>; therefore, BCL-x<sub>S</sub> lacks the BH1 domain and part of the BH2 domain [39]. This difference confers to BCL-x<sub>S</sub> a different (and antagonist) role to that of BCL-x<sub>L</sub>. All peptides identified in this experiment shared 100% homology with BCL-x<sub>L</sub> and importantly, two peptides (three and five) do not align with BCL-x<sub>S</sub>. Overall, 37% coverage of the BCL-x<sub>L</sub> protein was achieved, including coverage of the BH1, BH3, and BH4 domains, which play a key role in the interaction with other members of the BCL-2 family [40] (Supplementary Figure S2).

Calculation of the average intensity across all samples, as well as analysis of the number of BCL-x<sub>L</sub> peptides identified per sample (Supplementary Tables S2 and S3, respectively), revealed that a minimum of three peptides per replicate were detected in the IP samples, with intensities in the 10<sup>7</sup> range. In contrast, either zero or one BCL-x<sub>L</sub> peptides were identified in the negative controls, and when a peptide was detected, the corresponding intensity was low (~100× lower than in the immunoprecipitated samples).

Overall, BCL-x<sub>L</sub> was identified in immunoprecipitates prepared from uRBCs and iRBCs with a high level of confidence.

### 3.5. BCL-x<sub>L</sub> Forms Molecular Complexes with $\mu$ -Calpain in uRBCs and with SHOC2 in iRBCs

Assuming that WEHI-539 displaces host BCL-x<sub>L</sub> molecular complexes, the proteomics data set was analysed to identify proteins present in the BCL-x<sub>L</sub> IP sample without an inhibitor (i.e., BCL-x<sub>L</sub> binding partners), but absent or in low abundance in the BCL-x<sub>L</sub> IP with an inhibitor (i.e., BCL-x<sub>L</sub> displaced complexes). All proteins identified in the controls (i.e., extracts incubated with beads alone without BCL-x<sub>L</sub> antibody) were excluded.

In uRBCs,  $\mu$ -calpain (also called calpain-1), was identified in all three biological replicates from the uRBC-IP samples (i.e., uRBCs incubated with DMSO). However,  $\mu$ -calpain was not detected in any of the four biological replicates from the uRBC-IP + inhibitor samples (i.e., uRBCs incubated with the BCL-x<sub>L</sub> inhibitor WEHI-539) (Table 2). Therefore, this analysis identified  $\mu$ -calpain as a specific BCL-x<sub>L</sub> binding partner in uRBCs.

Conversely, in iRBCs, the human protein SHOC2, a leucine-rich repeat scaffold protein, was identified in three of the five independently generated iRBC-IP samples (i.e., iRBCs incubated with DMSO) but was not detected in any of the four BCL-x<sub>L</sub> immunoprecipitates derived from iRBC-IP + inhibitor samples (i.e., iRBCs incubated with the BCL-x<sub>L</sub> inhibitor WEHI-539) (Table 3). Therefore, human SHOC2 appears to form a molecular complex with host BCL-x<sub>L</sub> in iRBCs. Further, the interaction between SHOC2 and BCL-x<sub>L</sub> is specific to *P. falciparum* infection as SHOC2 was not immunoprecipitated in any of the uRBCs samples. Moreover, parasite proteins were also identified in the iRBC-IP samples, including the subunit D of a V-type proton ATPase, a pre-mRNA splicing factor, the pyrroline-5-carboxylate reductase, and the Apical sushi protein (Table 3). However, these proteins could only be detected in two or three of the five independent biological replicates, and with average intensities much lower than those obtained for the human proteins (i.e., the average intensity of the V-type proton ATPase is  $\sim 10\times$  lower than that of the human SHOC2). Therefore, the *P. falciparum* proteins identified in the iRBC-IP samples do not represent convincing binding partner candidates of BCL-x<sub>L</sub>.

**Table 2. BCL-x<sub>L</sub> binding partners identified in uRBCs.** Mass spectrometry analysis of BCL-x<sub>L</sub> immunoprecipitates from uRBCs with and without the BCL-x<sub>L</sub> inhibitor WEHI-539 over three and four independent biological replicates, respectively ( $n = 3-4$ ). The number of replicates in which the protein was identified is indicated, along with its relative average intensity.

Protein	Gene Name	uRBC-IP ( $n = 3$ )	Average Intensity	uRBC-IP + Inhibitor ( $n = 4$ )	Average Intensity
Calpain-1 catalytic subunit	CAPN1	3	1,268,283	0	N/A
E3 ubiquitin-protein ligase ARIH2	ARIH2	2	787,200	0	N/A
Mannose-1-phosphate guanyltransferase	GMPPA	2	584,955	0	N/A
Biliverdin reductase A	BLVRA	2	576,585	1	355,100

**Table 3. BCL-x<sub>L</sub> binding partners identified in iRBCs.** Mass spectrometry analysis of BCL-x<sub>L</sub> immunoprecipitates from iRBCs over a minimum of four independent biological replicates for each condition (iRBC-IP  $n = 4$ , iRBC-IP with inhibitor  $n = 5$ ). The number of replicates in which the protein was identified is indicated, along with its relative average intensity.

Human Proteins					
Protein	Gene Name	iRBC-IP ( $n = 5$ )	Average Intensity	iRBC-IP + Inhibitor ( $n = 4$ )	Average Intensity
Leucine-rich repeat protein SHOC-2	SHOC2	3	21,690,633	0	N/A
Hydroxyacylglutathione hydrolase, mitochondrial	HAGH	2	3,275,720	0	N/A
T-complex protein 1 subunit zeta-2	CCT6B	2	1,400,900	0	N/A
Annexin	ANXA1	2	583,760	0	N/A

Table 3. Cont.

Protein	Gene ID	<i>Plasmodium</i> Proteins			
		iRBC-IP (n = 5)	Average Intensity	iRBC-IP + Inhibitor (n = 4)	Average Intensity
V-type proton ATPase subunit D	PF3D7_1341900	2	1,245,405	0	N/A
Pre-mRNA splicing factor	PF3D7_0922700	2	751,780	0	N/A
Pyrroline-5-carboxylate reductase	PF3D7_1357900	3	499,970	0	N/A
Apical sushi protein, ASP	PF3D7_0405900	2	371,175	0	N/A

#### 4. Discussion

##### 4.1. Host BCL-x<sub>L</sub> Inhibition Impairs *P. falciparum* Growth

We have demonstrated that six BCL-x<sub>L</sub> inhibitors impair *in vitro* proliferation of *P. falciparum*. In particular, the FDA-approved drug ABT-199 displayed an IC<sub>50</sub> of 4.6 µM against parasite proliferation, which is within the range of the peak plasma concentrations found in patients treated for chronic lymphocytic leukaemia (CLL) or small lymphocytic lymphoma (SLL) [30]. Of note, anti-malarial drugs are generally found in the plasma at higher concentrations than their measured *in vitro* IC<sub>50</sub> values, so *in vivo* studies will be required to investigate ABT-199 bioavailability before progressing toward clinical evaluation for malaria treatment.

Two other BCL-x<sub>L</sub> inhibitors tested in this study, ABT-263, a drug currently in clinical trials for solid tumours [25,41], and WEHI-539, a highly specific inhibitor of BCL-x<sub>L</sub>, displayed the lowest *P. falciparum* IC<sub>50</sub> values of 0.74 and 0.82 µM, respectively. This IC<sub>50</sub> value of ABT-263 was around two- to eight-fold lower than the peak plasma concentrations measured following oral administration in an escalation study in humans [25]; however, future studies to measure plasma protein binding and free drug levels in plasma will be highly relevant to determine if this molecule can be further considered. Importantly, ABT-199 and ABT-263 half-lives are 19 h and 15 h, respectively. This feature is particularly attractive in the context of artemisinin-combination therapies where partner drugs (considering ABT-199 and ABT-263 in this case) are required to have longer half-lives than those of the artemisinins (i.e., greater than 10 h) [25,30,42]. This suggests that the pharmacokinetics of ABT-199 and ABT-263 may be sufficient to support further evaluation of the *in vivo* antimalarial efficacy of these candidates.

Interestingly, ABT-737 was previously found to impair the development of *P. yoelii* liver stages by inducing apoptosis of infected hepatocytes [11]. Similar to these previous findings, we demonstrated that BCL-x<sub>L</sub> inhibitors induce PS exposure in iRBCs, more so than in uRBCs (Figure 2). These findings are in agreement with another previous study where inhibition of BCL-x<sub>L</sub> with a BH3 peptide induced RBC death [13]. Of note, the three most specific inhibitors of BCL-x<sub>L</sub> (WEHI-539, A-155463 and A-1331852) significantly induced eryptosis of uRBCs, while the other three did not (Figure 2). Taken together, our data indicate that BCL-x<sub>L</sub> may play a role in eryptosis, although the molecular basis of this mechanism remains to be investigated.

*P. falciparum* has not been found to express BCL-x<sub>L</sub> orthologs [43], suggesting that the BCL-x<sub>L</sub> inhibitors tested in the present study act through the inhibition of host RBC factors, although off-target effects on other parasite proteins cannot be excluded at this stage. In human cells, some of the BCL-x<sub>L</sub> inhibitors tested here also target other members of the BCL-2 family (BCL-2, BCL-x and BCL-w) in the nanomolar range (Table 1). Given that the *P. falciparum* inhibitory concentrations tested in this study were in the micromolar range, we cannot exclude the possibility that the antiparasitic activity observed is due to the inhibition of members of the BCL-2 family other than BCL-x<sub>L</sub>. However, BCL-2 is yet to be identified in RBCs, suggesting that the ABT compounds tested act through the specific inhibition of BCL-x<sub>L</sub>. In future, the use of reverse genetics to impair the expression of specific proteins in the erythroid lineage [44], prior to infection with *Plasmodium* spp., would assist in investigating off-target effects and formally assign a role for BCL-x<sub>L</sub> in

infection. Overall, we report that BCL-x<sub>L</sub> inhibitors strongly impair the development of *P. falciparum* parasites *in vitro*.

#### 4.2. BCL-x<sub>L</sub> Is Recruited to the Parasite upon Infection

Considering that, in nucleated cells, the role of BCL-x<sub>L</sub> is highly dependent on its cellular localization [34], we investigated the cellular localization of BCL-x<sub>L</sub> in uRBCs and iRBCs and established that BCL-x<sub>L</sub> is strictly cytosolic in uRBCs (Figure 3A). Our Western blot analysis revealed a stronger signal of the protein 4.1 in the membrane fraction of iRBCs compared to all other fractions (Figure 3A, middle panel). One possible explanation is that protein 4.1 associates with other human and/or parasite membrane proteins in iRBCs, although this would need to be further investigated. Regardless, CA-I and PfHSP70.1 panels demonstrated an equal load of proteins in each lane, therefore validating the detection of BCL-x<sub>L</sub> in the membrane fraction of iRBCs. Of note, BCL-x<sub>L</sub> has been previously reported as a membrane protein in RBCs [13]; however, in this study, the membrane fraction was not controlled for the presence of cytosolic proteins. Therefore, contamination of the membrane fraction by cytosolic BCL-x<sub>L</sub> cannot be excluded.

Upon *P. falciparum* infection of RBCs, we have demonstrated that BCL-x<sub>L</sub> continues to localize to the host RBC cytosol but that a pool of the protein relocates either to the parasitophorous vacuole membrane, the parasite membrane, or within the parasite itself (Figure 3). *P. falciparum* is known to export a considerable number of proteins to its host cell, including many targeted to the RBC membrane, but only a few examples of functional human proteins have been shown to be imported by the parasite [45–48]. Further work is required to identify the exact subcellular localization of BCL-x<sub>L</sub> in iRBCs, and similar investigations should be carried out in infected hepatocytes. The BCL-x<sub>L</sub> transmembrane domain (TM) has been shown to be a bona fide targeting signal for the mitochondria's outer membrane [49]. Therefore, testing the competency of the BCL-x<sub>L</sub> TM as a targeting signal to the parasitophorous vacuole membrane (or the parasite membrane) would consolidate our findings.

#### 4.3. Identification of Novel BCL-x<sub>L</sub> Binding Partners in RBCs

The classical binding partners of BCL-x<sub>L</sub> (BAK, BAX, and BAD) have not been identified in RBCs in the current study following immunoprecipitation and mass spectrometry analyses. Instead, we found that BCL-x<sub>L</sub> forms a molecular complex with the human protein  $\mu$ -calpain in uRBCs and a complex with the human protein SHOC2 in iRBCs. Interestingly, the BCL-x<sub>L</sub> molecular complexes formed in uRBCs (Table 2) are distinct to those formed in iRBCs (Table 3), highlighting the effect of *Plasmodium* infection on host factors and the existence of a host–parasite molecular crosstalk. Further, as the current investigations focused on the analysis of trophozoite stages, the nature of BCL-x<sub>L</sub> molecular complexes should be investigated across the erythrocytic cycle (i.e., during ring and schizont stages).

Both the interactions of BCL-x<sub>L</sub> with  $\mu$ -calpain (in uRBCs) and with SHOC2 (in iRBCs) were disrupted in the presence of the BCL-x<sub>L</sub> inhibitor WEHI-539, suggesting that both proteins bind to BCL-x<sub>L</sub> via its BH3 domain. In addition, other BCL-x<sub>L</sub> binding partners not displaced by the presence of the inhibitor WEHI-539 have also been identified (Supplementary Tables S4 and S5). Presumably, such proteins bind to BCL-x<sub>L</sub> outside of the BH3 domain. However, in this case, peptides were typically only identified in less than half of the replicates, at relatively low intensities, and many such proteins are not biologically relevant (e.g., human nuclear proteins). Therefore, the validity of such BCL-x<sub>L</sub> binding partners warrants further investigation.

The most prominent BCL-x<sub>L</sub> binding partner identified in RBCs in this study is  $\mu$ -calpain (or calpain-1).  $\mu$ -Calpain is a calcium-dependent cysteine protease involved in the cleavage of cytoskeletal proteins in apoptosis and eryptosis [50,51]. In platelets,  $\mu$ -calpain also plays a role in the release of extracellular vesicles, exposing PS during platelet death induced by BCL-x<sub>L</sub> inhibitors [52]. Of note,  $\mu$ -calpain has been proposed to cleave the N-terminal end of BCL-x<sub>L</sub> [53] (although this is disputed, and this cleavage

is more often attributed to caspases [54,55]). The resulting cleaved-BCL-x<sub>L</sub> is proposed to induce apoptosis. Western blot analysis conducted in this study did not detect cleaved BCL-x<sub>L</sub> in either the uRBC or iRBC samples, despite the 16 kDa band being detected in the control sample (Figure 3), implying that  $\mu$ -calpain binds to BCL-x<sub>L</sub> in uRBCs without inducing protein cleavage. In addition to its role in cell death,  $\mu$ -calpain has been shown to be hijacked by *P. falciparum* to assist with egress from the host RBC, with a re-localization from the RBC cytosol to the parasite membrane during the schizont stage [56], although BCL-x<sub>L</sub> was not described to be involved.

The human protein SHOC2 was identified as a specific binding partner of BCL-x<sub>L</sub> in iRBCs, as this study demonstrated that the BCL-x<sub>L</sub>-SHOC2 complex is disrupted by the BCL-x<sub>L</sub> inhibitor WEHI-539 (Table 3). Noteworthy, SHOC2 was not found to bind to BCL-x<sub>L</sub> in uRBCs (Table 2, Supplementary Table S4). These findings suggest that upon invasion, a BCL-x<sub>L</sub>-SHOC2 complex may perform a specific function relevant for parasite development.

SHOC2 is a scaffold protein containing many leucine-rich repeats that mediate protein-protein interactions. However, the role of SHOC2 in human RBCs remains unknown. In mice, *shoc2* knock-out leads to early embryonic lethality, and in zebra fish, its deletion results in important defects in erythropoiesis, suggesting a role of SHOC2 in RBC generation [57]. In nucleated cells, SHOC2 was found to be a positive regulator in the RAS/ERK/MEK kinase signalling cascade (or the Mitogen-Activated Protein Kinase, MAPK pathway) [58]. Interestingly, it has been previously shown that *P. falciparum* relies on host proteins within the MAPK pathway for its development, namely MEK [59] and Raf [60]. In the context of cancer treatment, it was found that a combination of BCL-x<sub>L</sub> inhibitors together with MEK inhibitors could be efficient against KRAS mutant cancer models [61], highlighting cross-talk between the MAPK and the mitochondrion-dependent apoptosis pathways. However, the connection identified between these two pathways was the pro-apoptotic protein BIM, which to our knowledge has not yet been detected in RBCs. SHOC2 was also recently linked to DNA-damage-induced apoptosis, with *shoc2* knockdown affecting the BCL-2/BAX ratio (but no data on BCL-x<sub>L</sub> were included in this study) [62]. Overall, our data are consistent with previous studies showing that the MAPK pathway is particularly important in *P. falciparum*-iRBCs and implicate BCL-x<sub>L</sub> as a potential modulator of this pathway.

## 5. Conclusions

We have demonstrated that the inhibition of the host RBC BCL-x<sub>L</sub> protein impairs *P. falciparum* growth *in vitro* and that the BCL-x<sub>L</sub> inhibitors ABT-199 (an FDA-approved drug) and ABT-263 (a drug in clinical trials for solid tumours) display low micromolar and a submicromolar activity against the parasite, respectively. We have demonstrated that BCL-x<sub>L</sub> is exclusively cytosolic in uRBCs but becomes recruited to the parasite/parasitophorous vacuole upon infection. Finally, we discovered that BCL-x<sub>L</sub> forms novel molecular complexes in RBCs:  $\mu$ -calpain was shown to interact with BCL-x<sub>L</sub> in uRBCs, while SHOC2 binds to BCL-x<sub>L</sub> in iRBCs. Although the functionality of BCL-x<sub>L</sub> complexes in iRBCs remains to be fully elucidated, these complexes appear to play a key role in the development of *P. falciparum* inside human RBCs. Such findings present exciting possibilities for novel host pathways required for parasite development. Taken together, our findings suggest an important and novel role for human BCL-x<sub>L</sub> in *P. falciparum* development. Although the role of human BCL-x<sub>L</sub> both in uRBCs and in the development of *P. falciparum* remains unclear, we propose that BCL-x<sub>L</sub> inhibition represents an interesting and novel antimalarial strategy, which would allow (i) host-targeted therapy opportunities, (ii) drug repurposing, and (iii) simultaneous targeting of parasite hepatic and blood stages.

**Supplementary Materials:** The following are available online at <https://www.mdpi.com/article/10.3390/microorganisms10040824/s1>, **Figure S1: BCL-x<sub>L</sub> was successfully immunoprecipitated from uRBCs and iRBCs.** Western blot of BCL-x<sub>L</sub> immunoprecipitates from uRBCs and iRBCs previously exposed to BCL-x<sub>L</sub> inhibitor WEHI-539, or to vehicle DMSO, for 4 h at 37 °C. Controls are uRBC and iRBC protein extracts incubated with beads alone (no BCL-x<sub>L</sub> antibody). A tenth

of the total immunoprecipitation for each sample was analysed by Western blot, which was probed with 1:1000 anti-BCL-x<sub>L</sub> (Cell Signaling #2764). Ab: bands corresponding to the BCL-x<sub>L</sub> antibody. **Figure S2: BCL-x<sub>L</sub> peptides identified by mass spectrometry aligned over BCL-x<sub>L</sub>.** A. Schematic representation of BCL-x<sub>L</sub> peptides identified by mass spectrometry (Supplementary Table S1) aligned over the BCL-x<sub>L</sub> protein, including some important features of BCL-x<sub>L</sub>, namely: BH1, BH2, BH3, and BH4 domains, transmembrane domain, phosphorylation sites, and cleavage sites. B. Coverage of the BCL-x<sub>L</sub> protein identified by mass spectrometry. Over a total of 233 amino acids, 86 amino acids were identified (peptide sequences highlighted in blue), corresponding to a 37% protein coverage. **Table S1: BCL-x<sub>L</sub> peptides identified in RBC immunoprecipitation.** BCL-x<sub>L</sub> immunoprecipitation from uRBC and iRBC samples (+/– inhibitor WEHI-539) were analysed by mass spectrometry. Peptides corresponding to gene *bcl2-l1* are shown here with their amino acid sequences and length. These peptides were aligned to the BCL-x<sub>L</sub> amino acid sequence (using BLAST NCBI): the total score (alignment score) is calculated by giving a value to each aligned amino acid and summing these over the length of the peptide sequence. The E value, or Expected value, represents ‘the number of hits one can “expect” to see by chance when searching a database of a particular size’ (NCBI). All peptides shared 100% homology with a BCL-x<sub>L</sub> sequence. The number of times each peptide was detected (and over how many different conditions, i.e., uRBC or iRBC IP +/- inhibitor over several replicates) is indicated. **Table S2: BCL-x<sub>L</sub> peptides of BCL-x<sub>L</sub> immunoprecipitates from uRBCs.** Mass spectrometry analysis of BCL-x<sub>L</sub> immunoprecipitates from uRBCs: control (beads alone, no BCL-x<sub>L</sub> antibody; *n* = 2), uRBC-IP (*n* = 3), uRBC-IP + inhibitor WEHI-539 (*n* = 4). Number of BCL-x<sub>L</sub> peptides and the proteins’ average intensities in independent replicates are shown. **Table S3: BCL-x<sub>L</sub> peptides of BCL-x<sub>L</sub> immunoprecipitates from iRBCs.** Mass spectrometry analysis of BCL-x<sub>L</sub> immunoprecipitates from iRBCs: control (beads alone, no BCL-x<sub>L</sub> antibody; *n* = 3), uRBC-IP (*n* = 5), and uRBC-IP + inhibitor WEHI-539 (*n* = 4). Number of BCL-x<sub>L</sub> peptides and the proteins’ average intensities in independent replicates are shown. **Table S4: Proteins detected in BCL-x<sub>L</sub> immunoprecipitates from uRBCs, both with and without BCL-x<sub>L</sub> inhibitor WEHI-539.** Mass spectrometry analysis of BCL-x<sub>L</sub> immunoprecipitates from uRBCs without inhibitor (*n* = 3) and in the presence of inhibitor (*n* = 4). The number of replicates in which the protein was identified is indicated, along with its relative average intensity. **Table S5: Proteins detected in BCL-x<sub>L</sub> immunoprecipitates from iRBCs, both with and without BCL-x<sub>L</sub> inhibitor WEHI-539.** Mass spectrometry analysis of BCL-x<sub>L</sub> immunoprecipitates from iRBCs without inhibitor (*n* = 5) and in the presence of inhibitor (*n* = 4). The number of replicates in which the protein was identified is indicated, along with its average intensity.

**Author Contributions:** Conceptualization, C.B. and T.G.C.; resources, T.G.C., D.J.C. and C.D.; project administration, T.G.C.; funding acquisition, T.G.C.; experiments, C.B., T.L.G., G.S. and T.G.C.; methodology, C.B., G.S. and T.G.C.; data curation, C.B., G.S. and T.G.C.; supervision, D.J.C. and T.G.C.; writing—original draft preparation, C.B. and T.G.C.; writing—reviewing and editing, C.B., G.S., T.L.G., C.D., D.J.C. and T.G.C. All authors have read and agreed to the published version of the manuscript.

**Funding:** This research was funded by La Trobe University, via an internal competitive funding scheme awarded to T.G.C. (grant number 315011737) and a 3-year post-graduate PhD Scholarship awarded to C.B.

**Institutional Review Board Statement:** Not applicable.

**Informed Consent Statement:** Not applicable.

**Data Availability Statement:** All the raw data and search result files (MaxQuant excel output) for the IP experiments have been deposited in the ProteomeXchange Consortium through the PRIDE partner repository [63] with identifier PXD032276. Username: reviewer\_pxd032276@ebi.ac.uk, Password: MgxKbYII.

**Acknowledgments:** We acknowledge the traditional custodians of the lands this project was conducted on: the Wurundjeri people of the Kulin Nation. We thank Delphine Merino (Olivia Newton-John Cancer Research Centre) for providing MDA-MB-231 protein extracts and for her advice on BCL-x<sub>L</sub> inhibitors. We thank Simona John von Freyend (Monash University) for her assistance with Western blots, Leanne Tilley and Mathew Dixon (University of Melbourne) for microscopy support,

and Chad Johnson (Bioimaging Platform, La Trobe University) for imaging assistance. We thank the Australian Red Cross for the regular supply of human red blood cells.

**Conflicts of Interest:** The authors declare no conflict of interest.

## References

1. WHO. World Malaria Report. 2021. Available online: <https://www.who.int/publications-detail-redirect/9789240040496> (accessed on 19 January 2022).
2. WHO. Malaria Eradication: Benefits, Future Scenarios & Feasibility. Available online: <https://www.who.int/publications-detail-redirect/9789240003675> (accessed on 19 January 2022).
3. Laurens, M.B. RTS,S/AS01 Vaccine (Mosquirix™): An Overview. *Hum. Vaccin Immunother.* **2019**, *16*, 480–489. [[CrossRef](#)] [[PubMed](#)]
4. RTS,S Clinical Trials Partnership. Efficacy and Safety of RTS,S/AS01 Malaria Vaccine with or without a Booster Dose in Infants and Children in Africa: Final Results of a Phase 3, Individually Randomised, Controlled Trial. *Lancet* **2015**, *386*, 31–45. [[CrossRef](#)]
5. Noedl, H.; Se, Y.; Schaefer, K.; Smith, B.L.; Socheat, D.; Fukuda, M.M. Artemisinin Resistance in Cambodia 1 (ARC1) Study Consortium Evidence of Artemisinin-Resistant Malaria in Western Cambodia. *N. Engl. J. Med.* **2008**, *359*, 2619–2620. [[CrossRef](#)] [[PubMed](#)]
6. Glennon, E.K.K.; Dankwa, S.; Smith, J.D.; Kaushansky, A. Opportunities for Host-Targeted Therapies for Malaria. *Trends Parasitol.* **2018**, *34*, 843–860. [[CrossRef](#)]
7. Wei, L.; Adderley, J.; Leroy, D.; Drewry, D.H.; Wilson, D.W.; Kaushansky, A.; Doerig, C. Host-Directed Therapy, an Untapped Opportunity for Antimalarial Intervention. *Cell Rep. Med.* **2021**, *2*, 100423. [[CrossRef](#)] [[PubMed](#)]
8. Carneiro, B.A.; El-Deiry, W.S. Targeting Apoptosis in Cancer Therapy. *Nat. Rev. Clin. Oncol.* **2020**, *17*, 395–417. [[CrossRef](#)]
9. Chakraborty, S.; Roy, S.; Mistry, H.U.; Murthy, S.; George, N.; Bhandari, V.; Sharma, P. Potential Sabotage of Host Cell Physiology by Apicomplexan Parasites for Their Survival Benefits. *Front. Immunol.* **2017**, *8*, 1261. [[CrossRef](#)]
10. van de Sand, C.; Horstmann, S.; Schmidt, A.; Sturm, A.; Bolte, S.; Krueger, A.; Lütgehetmann, M.; Pollok, J.-M.; Libert, C.; Heussler, V.T. The Liver Stage of Plasmodium Berghei Inhibits Host Cell Apoptosis. *Mol. Microbiol.* **2005**, *58*, 731–742. [[CrossRef](#)]
11. Kaushansky, A.; Metzger, P.G.; Douglass, A.N.; Mikolajczak, S.A.; Lakshmanan, V.; Kain, H.S.; Kappe, S.H. Malaria Parasite Liver Stages Render Host Hepatocytes Susceptible to Mitochondria-Initiated Apoptosis. *Cell Death Dis.* **2013**, *4*, e762. [[CrossRef](#)] [[PubMed](#)]
12. Roux-Dalvai, F.; Gonzalez de Peredo, A.; Simó, C.; Guerrier, L.; Bouyssié, D.; Zanella, A.; Citterio, A.; Bulet-Schiltz, O.; Boschetti, E.; Righetti, P.G.; et al. Extensive Analysis of the Cytoplasmic Proteome of Human Erythrocytes Using the Peptide Ligand Library Technology and Advanced Mass Spectrometry. *Mol. Cell Proteom.* **2008**, *7*, 2254–2269. [[CrossRef](#)] [[PubMed](#)]
13. Walsh, M.; Lutz, R.J.; Cotter, T.G.; O'Connor, R. Erythrocyte Survival Is Promoted by Plasma and Suppressed by a Bak-Derived BH3 Peptide That Interacts with Membrane-Associated Bcl-X(L). *Blood* **2002**, *99*, 3439–3448. [[CrossRef](#)] [[PubMed](#)]
14. Bratosin, D.; Estaquier, J.; Petit, F.; Arnoult, D.; Quatannens, B.; Tissier, J.P.; Slomianny, C.; Sartiaux, C.; Alonso, C.; Huart, J.J.; et al. Programmed Cell Death in Mature Erythrocytes: A Model for Investigating Death Effector Pathways Operating in the Absence of Mitochondria. *Cell Death Differ.* **2001**, *8*, 1143–1156. [[CrossRef](#)]
15. Trager, W.; Jensen, J.B. Human Malaria Parasites in Continuous Culture. *Science* **1976**, *193*, 673–675. [[CrossRef](#)]
16. Boulet, C.; Gaynor, T.L.; Carvalho, T.G. Eryptosis and Malaria: New Experimental Guidelines and Re-Evaluation of the Antimalarial Potential of Eryptosis Inducers. *Front. Cell Infect. Microbiol.* **2021**, *11*, 630812. [[CrossRef](#)]
17. Lambros, C.; Vanderberg, J.P. Synchronization of Plasmodium Falciparum Erythrocytic Stages in Culture. *J. Parasitol.* **1979**, *65*, 418–420. [[CrossRef](#)] [[PubMed](#)]
18. Ribaut, C.; Berry, A.; Chevalley, S.; Reybier, K.; Morlais, I.; Parzy, D.; Nepveu, F.; Benoit-Vical, F.; Valentin, A. Concentration and Purification by Magnetic Separation of the Erythrocytic Stages of All Human Plasmodium Species. *Malar. J.* **2008**, *7*, 45. [[CrossRef](#)]
19. Siddiqui, G.; De Paoli, A.; MacRaild, C.A.; Sexton, A.E.; Boulet, C.; Shah, A.D.; Batty, M.B.; Schittenhelm, R.B.; Carvalho, T.G.; Creek, D.J. A New Mass Spectral Library for High-Coverage and Reproducible Analysis of the Plasmodium Falciparum-Infected Red Blood Cell Proteome. *GigaScience* **2022**, *11*, giac008. [[CrossRef](#)] [[PubMed](#)]
20. Ansoorge, I.; Benting, J.; Bhakdi, S.; Lingelbach, K. Protein Sorting in Plasmodium Falciparum-Infected Red Blood Cells Permeabilized with the Pore-Forming Protein Streptolysin O. *Biochem. J.* **1996**, *315 Pt 1*, 307–314. [[CrossRef](#)]
21. Wang, M.; Siddiqui, G.; Gustafsson, O.J.R.; Käkinen, A.; Javed, I.; Voelcker, N.H.; Creek, D.J.; Ke, P.C.; Davis, T.P. Plasma Proteome Association and Catalytic Activity of Stealth Polymer-Grafted Iron Oxide Nanoparticles. *Small* **2017**, *13*, 1701528. [[CrossRef](#)]
22. Siddiqui, G.; Srivastava, A.; Russell, A.S.; Creek, D.J. Multi-Omics Based Identification of Specific Biochemical Changes Associated With PfKelch13-Mutant Artemisinin-Resistant Plasmodium Falciparum. *J. Infect. Dis.* **2017**, *215*, 1435–1444. [[CrossRef](#)]
23. Nandakumar, A.; Wei, W.; Siddiqui, G.; Tang, H.; Li, Y.; Käkinen, A.; Wan, X.; Koppel, K.; Lin, S.; Davis, T.P.; et al. Dynamic Protein Corona of Gold Nanoparticles with an Evolving Morphology. *ACS Appl. Mater. Interfaces* **2021**, *13*, 58238–58251. [[CrossRef](#)]
24. Park, C.-M.; Bruncko, M.; Adickes, J.; Bauch, J.; Ding, H.; Kunzer, A.; Marsh, K.C.; Nimmer, P.; Shoemaker, A.R.; Song, X.; et al. Discovery of an Orally Bioavailable Small Molecule Inhibitor of Prosurvival B-Cell Lymphoma 2 Proteins. *J. Med. Chem.* **2008**, *51*, 6902–6915. [[CrossRef](#)] [[PubMed](#)]

25. Gandhi, L.; Camidge, D.R.; Ribeiro de Oliveira, M.; Bonomi, P.; Gandara, D.; Khaira, D.; Hann, C.L.; McKeegan, E.M.; Litvinovich, E.; Hemken, P.M.; et al. Phase I Study of Navitoclax (ABT-263), a Novel Bcl-2 Family Inhibitor, in Patients with Small-Cell Lung Cancer and Other Solid Tumors. *J. Clin. Oncol.* **2011**, *29*, 909–916. [[CrossRef](#)]
26. Douglass, A.N.; Kain, H.S.; Abdullahi, M.; Arang, N.; Austin, L.S.; Mikolajczak, S.A.; Billman, Z.P.; Hume, J.C.C.; Murphy, S.C.; Kappe, S.H.I.; et al. Host-Based Prophylaxis Successfully Targets Liver Stage Malaria Parasites. *Mol. Ther.* **2015**, *23*, 857–865. [[CrossRef](#)] [[PubMed](#)]
27. Lessene, G.; Czabotar, P.E.; Sleeb, B.E.; Zobel, K.; Lowes, K.N.; Adams, J.M.; Baell, J.B.; Colman, P.M.; Deshayes, K.; Fairbrother, W.J.; et al. Structure-Guided Design of a Selective BCL-X(L) Inhibitor. *Nat. Chem. Biol.* **2013**, *9*, 390–397. [[CrossRef](#)] [[PubMed](#)]
28. Tao, Z.-F.; Hasvold, L.; Wang, L.; Wang, X.; Petros, A.M.; Park, C.H.; Boghaert, E.R.; Catron, N.D.; Chen, J.; Colman, P.M.; et al. Discovery of a Potent and Selective BCL-XL Inhibitor with in Vivo Activity. *ACS Med. Chem. Lett.* **2014**, *5*, 1088–1093. [[CrossRef](#)] [[PubMed](#)]
29. Souers, A.J.; Levenson, J.D.; Boghaert, E.R.; Ackler, S.L.; Catron, N.D.; Chen, J.; Dayton, B.D.; Ding, H.; Enschede, S.H.; Fairbrother, W.J.; et al. ABT-199, a Potent and Selective BCL-2 Inhibitor, Achieves Antitumor Activity While Sparing Platelets. *Nat. Med.* **2013**, *19*, 202–208. [[CrossRef](#)]
30. Roberts, A.W.; Davids, M.S.; Pagel, J.M.; Kahl, B.S.; Puvvada, S.D.; Gerecitano, J.F.; Kipps, T.J.; Anderson, M.A.; Brown, J.R.; Gressick, L.; et al. Targeting BCL2 with Venetoclax in Relapsed Chronic Lymphocytic Leukemia. *N. Engl. J. Med.* **2016**, *374*, 311–322. [[CrossRef](#)]
31. Oltersdorf, T.; Elmoe, S.W.; Shoemaker, A.R.; Armstrong, R.C.; Augeri, D.J.; Belli, B.A.; Bruncko, M.; Deckwerth, T.L.; Dinges, J.; Hajduk, P.J.; et al. An Inhibitor of Bcl-2 Family Proteins Induces Regression of Solid Tumours. *Nature* **2005**, *435*, 677–681. [[CrossRef](#)]
32. Levenson, J.D.; Phillips, D.C.; Mitten, M.J.; Boghaert, E.R.; Diaz, D.; Tahir, S.K.; Belmont, L.D.; Nimmer, P.; Xiao, Y.; Ma, X.M.; et al. Exploiting Selective BCL-2 Family Inhibitors to Dissect Cell Survival Dependencies and Define Improved Strategies for Cancer Therapy. *Sci. Transl. Med.* **2015**, *7*, 279ra40. [[CrossRef](#)]
33. Boulet, C.; Doerig, C.D.; Carvalho, T.G. Manipulating Eryptosis of Human Red Blood Cells: A Novel Antimalarial Strategy? *Front. Cell Infect. Microbiol.* **2018**, *8*, 419. [[CrossRef](#)]
34. Popgeorgiev, N.; Jabbour, L.; Gillet, G. Subcellular Localization and Dynamics of the Bcl-2 Family of Proteins. *Front. Cell Dev. Biol.* **2018**, *6*, 13. [[CrossRef](#)]
35. Ringrose, J.H.; van Solinge, W.W.; Mohammed, S.; O’Flaherty, M.C.; van Wijk, R.; Heck, A.J.R.; Slijper, M. Highly Efficient Depletion Strategy for the Two Most Abundant Erythrocyte Soluble Proteins Improves Proteome Coverage Dramatically. *J. Proteome Res.* **2008**, *7*, 3060–3063. [[CrossRef](#)]
36. Takakuwa, Y. Protein 4.1, a Multifunctional Protein of the Erythrocyte Membrane Skeleton: Structure and Functions in Erythrocytes and Nonerythroid Cells. *Int. J. Hematol.* **2000**, *72*, 298–309. [[PubMed](#)]
37. Pesce, E.-R.; Acharya, P.; Tatu, U.; Nicoll, W.S.; Shonhai, A.; Hoppe, H.C.; Blatch, G.L. The Plasmodium Falciparum Heat Shock Protein 40, Pf4, Associates with Heat Shock Protein 70 and Shows Similar Heat Induction and Localisation Patterns. *Int. J. Biochem. Cell Biol.* **2008**, *40*, 2914–2926. [[CrossRef](#)]
38. Czabotar, P.E.; Lessene, G.; Strasser, A.; Adams, J.M. Control of Apoptosis by the BCL-2 Protein Family: Implications for Physiology and Therapy. *Nat. Rev. Mol. Cell Biol.* **2014**, *15*, 49–63. [[CrossRef](#)]
39. Stevens, M.; Oltean, S. Modulation of the Apoptosis Gene Bcl-x Function Through Alternative Splicing. *Front. Genet.* **2019**, *10*, 804. [[CrossRef](#)]
40. Yin, X.M.; Oltvai, Z.N.; Veis-Novack, D.J.; Linette, G.P.; Korsmeyer, S.J. Bcl-2 Gene Family and the Regulation of Programmed Cell Death. *Cold Spring Harb. Symp. Quant. Biol.* **1994**, *59*, 387–393. [[CrossRef](#)] [[PubMed](#)]
41. AbbVie. *A Phase 1 Safety and Pharmacokinetic Study of ABT-263 in Combination with Paclitaxel in the Treatment of Subjects with Solid Tumors*; U.S. National Library of Medicine: Bethesda, MD, USA, 2017.
42. de Vries, P.J.; Dien, T.K. Clinical Pharmacology and Therapeutic Potential of Artemisinin and Its Derivatives in the Treatment of Malaria. *Drugs* **1996**, *52*, 818–836. [[CrossRef](#)] [[PubMed](#)]
43. PlasmoDB. Available online: <https://plasmodb.org/plasmo/app> (accessed on 19 January 2022).
44. Crosnier, C.; Bustamante, L.Y.; Bartholdson, S.J.; Bei, A.K.; Theron, M.; Uchikawa, M.; Mboup, S.; Ndir, O.; Kwiatkowski, D.P.; Duraisingh, M.T.; et al. Basigin Is a Receptor Essential for Erythrocyte Invasion by Plasmodium Falciparum. *Nature* **2011**, *480*, 534–537. [[CrossRef](#)] [[PubMed](#)]
45. Koncarevic, S.; Rohrbach, P.; Deponte, M.; Krohne, G.; Prieto, J.H.; Yates, J.; Rahlfs, S.; Becker, K. The Malarial Parasite Plasmodium Falciparum Imports the Human Protein Peroxiredoxin 2 for Peroxide Detoxification. *Proc. Natl. Acad. Sci. USA* **2009**, *106*, 13323–13328. [[CrossRef](#)] [[PubMed](#)]
46. Foth, B.J.; Zhang, N.; Chaal, B.K.; Sze, S.K.; Preiser, P.R.; Bozdech, Z. Quantitative Time-Course Profiling of Parasite and Host Cell Proteins in the Human Malaria Parasite Plasmodium Falciparum. *Mol. Cell Proteom.* **2011**, *10*, M110.006411. [[CrossRef](#)] [[PubMed](#)]
47. Tougan, T.; Edula, J.R.; Takashima, E.; Morita, M.; Shinohara, M.; Shinohara, A.; Tsuboi, T.; Horii, T. Molecular Camouflage of Plasmodium Falciparum Merozoites by Binding of Host Vitronectin to P47 Fragment of SERA5. *Sci. Rep.* **2018**, *8*, 5052. [[CrossRef](#)]
48. El Chamy Maluf, S.; Icimoto, M.Y.; Melo, P.M.S.; Budu, A.; Coimbra, R.; Gazarini, M.L.; Carmona, A.K. Human Plasma Plasminogen Internalization Route in Plasmodium Falciparum-Infected Erythrocytes. *Malar. J.* **2020**, *19*, 302. [[CrossRef](#)] [[PubMed](#)]

49. Kaufmann, T.; Schlipf, S.; Sanz, J.; Neubert, K.; Stein, R.; Borner, C. Characterization of the Signal That Directs Bcl-x(L), but Not Bcl-2, to the Mitochondrial Outer Membrane. *J. Cell Biol.* **2003**, *160*, 53–64. [[CrossRef](#)] [[PubMed](#)]
50. Perrin, B.J.; Huttenlocher, A. Calpain. *Int. J. Biochem. Cell Biol.* **2002**, *34*, 722–725. [[CrossRef](#)]
51. Berg, C.P.; Engels, I.H.; Rothbart, A.; Lauber, K.; Renz, A.; Schlosser, S.F.; Schulze-Osthoff, K.; Wesselborg, S. Human Mature Red Blood Cells Express Caspase-3 and Caspase-8, but Are Devoid of Mitochondrial Regulators of Apoptosis. *Cell Death Differ.* **2001**, *8*, 1197–1206. [[CrossRef](#)]
52. Wei, H.; Harper, M.T. Comparison of Putative BH3 Mimetics AT-101, HA14-1, Sabutoclax and TW-37 with ABT-737 in Platelets. *Platelets* **2021**, *32*, 105–112. [[CrossRef](#)]
53. Nakagawa, T.; Yuan, J. Cross-Talk between Two Cysteine Protease Families. Activation of Caspase-12 by Calpain in Apoptosis. *J. Cell Biol.* **2000**, *150*, 887–894. [[CrossRef](#)]
54. Tan, Y.; Dourdin, N.; Wu, C.; De Veyra, T.; Elce, J.S.; Greer, P.A. Conditional Disruption of Ubiquitous Calpains in the Mouse. *Genesis* **2006**, *44*, 297–303. [[CrossRef](#)]
55. Clem, R.J.; Cheng, E.H.; Karp, C.L.; Kirsch, D.G.; Ueno, K.; Takahashi, A.; Kastan, M.B.; Griffin, D.E.; Earnshaw, W.C.; Veluona, M.A.; et al. Modulation of Cell Death by Bcl-XL through Caspase Interaction. *Proc. Natl. Acad. Sci. USA* **1998**, *95*, 554–559. [[CrossRef](#)] [[PubMed](#)]
56. Chandramohanadas, R.; Davis, P.H.; Beiting, D.P.; Harbut, M.B.; Darling, C.; Velmourougane, G.; Lee, M.Y.; Greer, P.A.; Roos, D.S.; Greenbaum, D.C. Apicomplexan Parasites Co-Opt Host Calpains to Facilitate Their Escape from Infected Cells. *Science* **2009**, *324*, 794–797. [[CrossRef](#)] [[PubMed](#)]
57. Jang, H.; Oakley, E.; Forbes-Osborne, M.; Kesler, M.V.; Norcross, R.; Morris, A.C.; Galperin, E. Hematopoietic and Neural Crest Defects in Zebrafish Shoc2 Mutants: A Novel Vertebrate Model for Noonan-like Syndrome. *Hum. Mol. Genet.* **2019**, *28*, 501–514. [[CrossRef](#)] [[PubMed](#)]
58. Rodriguez-Viciania, P.; Osés-Prieto, J.; Burlingame, A.; Fried, M.; McCormick, F. A Phosphatase Holoenzyme Comprised of Shoc2/Sur8 and the Catalytic Subunit of PP1 Functions as an M-Ras Effector to Modulate Raf Activity. *Mol. Cell* **2006**, *22*, 217–230. [[CrossRef](#)]
59. Sicard, A.; Semblat, J.-P.; Doerig, C.; Hamelin, R.; Moniatte, M.; Dorin-Semblat, D.; Spicer, J.A.; Srivastava, A.; Retzlaff, S.; Heussler, V.; et al. Activation of a PAK-MEK Signalling Pathway in Malaria Parasite-Infected Erythrocytes. *Cell Microbiol.* **2011**, *13*, 836–845. [[CrossRef](#)]
60. Adderley, J.D.; Doerig, C. Erythrocyte Phospho-Signalling Is Dynamically Altered during Infection with Plasmodium Falciparum. *Microb. Cell* **2020**, *7*, 286–288. [[CrossRef](#)]
61. Corcoran, R.B.; Cheng, K.A.; Hata, A.N.; Faber, A.C.; Ebi, H.; Coffee, E.M.; Greninger, P.; Brown, R.D.; Godfrey, J.T.; Cohoon, T.J.; et al. Synthetic Lethal Interaction of Combined BCL-XL and MEK Inhibition Promotes Tumor Regressions in KRAS Mutant Cancer Models. *Cancer Cell* **2013**, *23*, 121–128. [[CrossRef](#)]
62. Silveira, V.S.; Borges, K.S.; Santos, V.S.; Ruckert, M.T.; Vieira, G.M.; Vasconcelos, E.J.R.; Nagano, L.F.P.; Tone, L.G.; Scrideli, C.A. SHOC2 Scaffold Protein Modulates Daunorubicin-Induced Cell Death through P53 Modulation in Lymphoid Leukemia Cells. *Sci. Rep.* **2020**, *10*, 15193. [[CrossRef](#)]
63. Perez-Riverol, Y.; Csordas, A.; Bai, J.; Bernal-Llinares, M.; Hewapathirana, S.; Kundu, D.J.; Inuganti, A.; Griss, J.; Mayer, G.; Eisenacher, M.; et al. The PRIDE Database and Related Tools and Resources in 2019: Improving Support for Quantification Data. *Nucleic Acids Res.* **2019**, *47*, D442–D450. [[CrossRef](#)]